Electrochemically Induced Synthesis of Triphenylamine-based Polyhydrazones

P. Data[a,b,c,1,*], P. Pander[a,b], P. Zassowski[b], V. Mimaite[d], K. Karon[b], M. Lapkowski[b,c], J.V. Grazulevicius[d], P. Slepski[e], K. Darowicki[e]

[a] Physics Department, Durham University, South Road, Durham, DH1 3LE, United Kingdom
[b] Faculty of Chemistry, Silesian University of Technology, M. Strzody 9, 44-100 Gliwice, Poland
[c] Center of Polymer and Carbon Materials, Polish Academy of Science, M. Curie-Sklodowskiej 34, 41-819 Zabrze, Poland
[d] Department of Polymer Chemistry and Technology, Kaunas University of Technology, Radvilenu pl. 19, LT-50254, Kaunas, Lithuania
[e] Department of Electrochemistry, Corrosion and Material Engineering, Faculty of Chemistry, Gdansk University of Technology, 11/12 Narutowicza St., 80 233 Gdansk, Poland

ARTICLE INFO

ABSTRACT

Triphenylamine-based hydrazones were subjected to electropolymerization process that gave well conductive hydrazone based polymers. The first example of polyhydrazone formation during the electrochemical process was shown. The estimation of polymer structure was demonstrated using IR spectroelectrochemistry. The EPR spectroelectrochemistry allowed to explain why in some cases dimer couldn't be formed. The results of electrochemical, spectroelectrochemical investigation of small molecules, as well as their polymers obtained by electropolymerization, are presented. The comparative study of electropolymerization and doping process by IR, EPR, potentiostatic and potentiodynamic UV-Vis-NIR, DEIS spectroelectrochemical techniques was performed to determine the reaction path, charge carriers and conductivity of polymeric layers.

1. Introduction

Hydrazones have been extensively studied in various fields ranging from organic synthesis [1–3], supramolecular chemistry [4–6], medicinal chemistry [7–10]. They have been used as dyes [11,12], hole-transporting materials [13,14], organic nonlinear optical materials [15] in metal and covalent organic frameworks [16–19], dynamic combinatorial chemistry (DCC) [20–22], dye-sensitized solar cells [23] and molecular switches [24]. The modularity, straightforward synthesis, and stability towards hydrolysis of hydrazones can be mentioned as the reasons for their popularity [14]. Hydrazones can be prepared by three main synthetic pathways: coupling between aryl diazonium salts and b-keto esters or acids, which is also known as the Japp–Klingemann reaction [25], coupling between hydrazines and ketones or aldehydes [26] and coupling between aryl halides and non-substituted hydrazones [27]. The readily obtained compounds are usually highly crystalline and precipitate out of the reaction mixture, which simplifies their purification process. Due to the simplicity of the synthesis and high charge carrier mobilities hydrazones play an important role among organic hole-transporting materials, especially those used in electrophotography [28,29]. Crystalline aromatic hydrazone molecules are not capable of forming thin, neat homogenous layers, and must be used in combination with polymeric hosts in use as the main constituent of electrophotographic devices or active layer in optoelectronic devices. Recently, new monomers [30,31] and polymers [32–34] based on dihydrazone moieties capable of yielding the polymeric hole transport layers were reported. These monomers and polymers exhibit high hole drift mobilities and good film-forming properties. All these polymers were synthetized in the polyaddition reaction with bifunctional nucleophilic linking agents in the presence of a catalyst. Some of them can be chemically cross-linked in the layer by reaction of the hydroxyl groups with polyisocyanates [35]. Such cross-linked systems [30] enable to prepare electrophotographic photoreceptors with high solvent resistance and good mechanical properties [36,37].

In this study, we investigated hydrazone derivatives (Fig. 1) that can be polymerized electrochemically giving conductive polymers. In recent years, many molecules containing hydrazone moiety and having electroactive properties were synthesized. They had
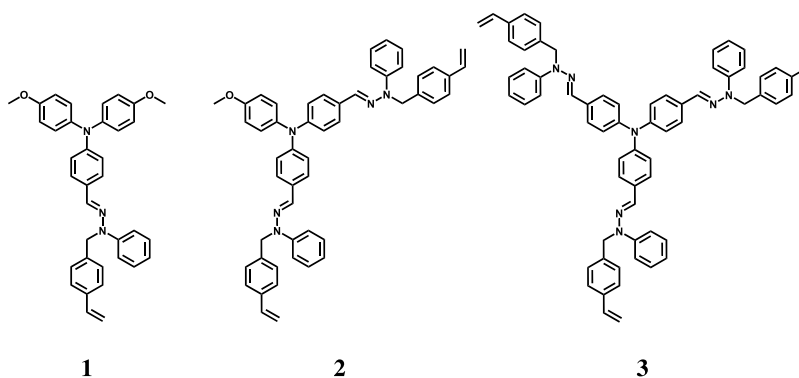
Fig. 1. The chemical structures of investigated compounds.

different electrophores, such phenothiazine [38], triphenylamine [39] or 3,4-ethylenedioxythiophene [40]. To the best of our knowledge, this is the first report on the preparation of conductive polymers by electrochemical polymerization of compounds containing hydrazone moieties. Molecules containing hydrazone moiety substituted by phenylene units are electroactive and have been the subjects of numerous electrochemical studies [41–43]. However, there are no reports of the synthesis of conducting polymers containing hydrazine species.

2. Experimental Section

2.1. Materials

The synthesis of the investigated compounds is reported in the literature [31]. All the solvents used for the measurements were dried and distilled before use. The commercial reagents were used without purification. Electrochemical measurements were done in 1.0 mM concentrations of all compounds for all the cyclic voltammetry measurements. Electrochemical studies were conducted in 0.1 M solutions of Bu_4NBF_4, 99% (Sigma-Aldrich) in dichloromethane (DCM) solvent, CHROMASOLV®, 99.9% (Sigma-Aldrich) at room temperature. UV–vis spectroelectrochemical measurements were performed on the ITO (Indium Tin Oxide) quartz glass working electrode coated with polymers.

2.2. Measurements

The electrochemical investigations were carried out using a potentiostats Autolab PGSTAT20 and Metrohm Autolab

PGSTAT100. The cyclic voltammetry (CV) measurements were performed with 1.0 mM solutions of compounds. Electrochemical studies were carried out using 0.1 M solutions of Bu_4NBF_4 in dichloromethane (DCM). The electrochemical cell consisted of 1 mm diameter platinum disk working electrode, Ag/AgCl electrode as a reference electrode and platinum coil as the auxiliary electrode. All electrodes were cleaned before use. The platinum working electrode was polished before use on a polishing pad with 1 μm alumina slurry, then the platinum electrode was rinsed with deionized water and cleaned in an ultrasound bath with deionized water for 15 minutes. After water cleaning the electrode was rinsed with isopropanol (3x), acetone (3x) and dried. The electrode was used directly after cleaning. CV measurements were conducted at room temperature at a potential rate of 50 mV/s and were calibrated against ferrocene/ferrocenium redox couple. UV-Vis-NIR spectroelectrochemical measurements were performed using Indium Tin Oxide (ITO) deposited on quartz glass substrate as the working electrode. Polymeric layers were synthesized on ITO electrode at the conditions similar to that of CV measurements. UV-Vis-NIR spectroscopy and spectroelectrochemistry experiments were performed using QE6500 and NIRQuest detectors (Ocean Optics). IR measurements were carried out using PerkinElmer Spectrum Two FT-IR Spectrometer equipped with UATR attachment with diamond crystal. The in situ IR-ATR-spectroelectrochemical measurements were done using vertical ZnSe crystal that was located between two opposite, large surface area electrodes forming with the crystal walls a thin-layer cavity. Electron paramagnetic resonance (EPR) measurements were performed using a JEOL JES-FA200 spectrometer coupled with an Autolab PGSTAT 100N potentiostat. Measurements were
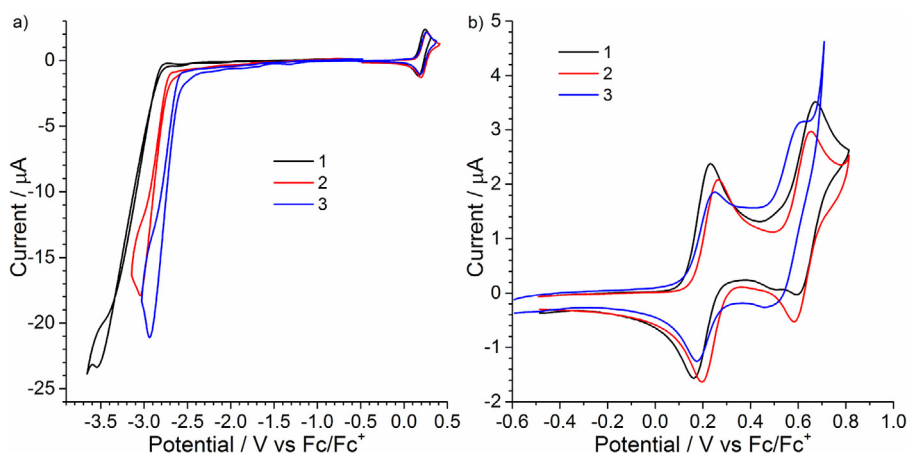

Fig. 2. CV curves of compounds **1**-**3** at broad oxidation reduction potential range (a) and oxidation range (b). Sample concentration 10^{-3} M, scan rate 0.05 V·s^{-1}, dichloromethane solution for oxidation and THF for reduction. All potentials vs Fc/Fc$^+$ redox couple.
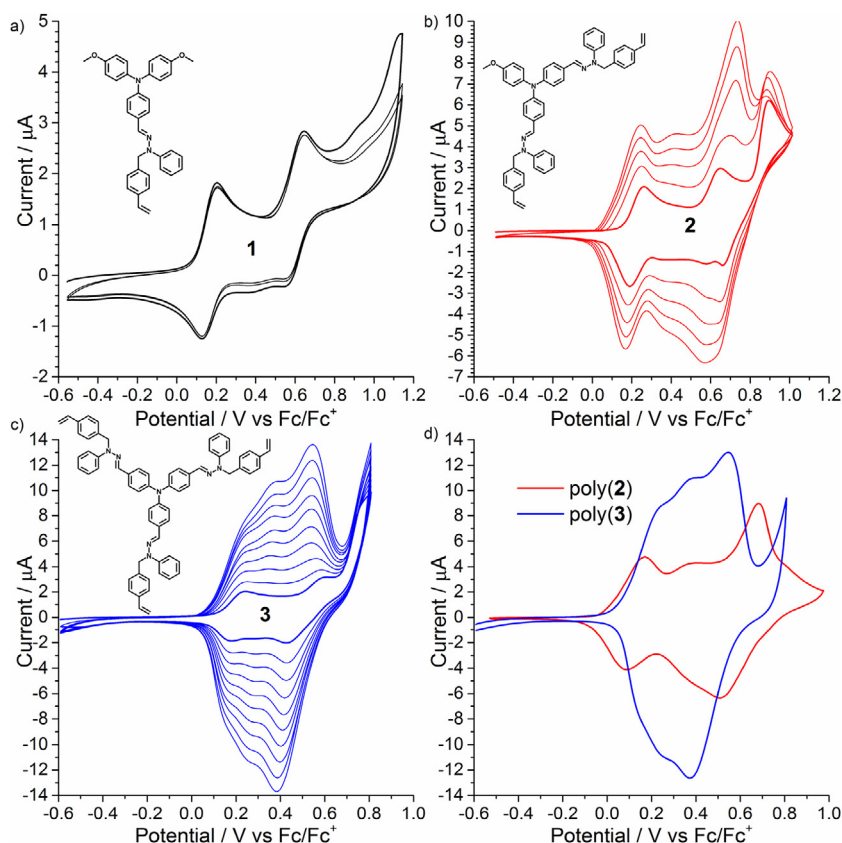
Fig. 3. CV curves of a) compound **1**, b-c) polymerization of compounds **2** and **3**, d) electrochemical doping-dedoping process of the polymers. Sample concentration 10^{-3} M, scan rate 0.05 V·s^{-1}, dichloromethane solution. All potentials vs Fc/Fc$^+$ redox couple.

performed in a spectroelectrochemical glass cell narrowed at the bottom to provide proper conditions for EPR spectra recording. The number of spins was estimated by double integration of obtained spectra. The g-factor of spins generated during the oxidation was determined by comparison with JEOL internal standard (Mn(II) salt), knowing that its third hyperfine line has a g-factor of 2.03323. The colorimetric analysis was performed on 80 mm integrating sphere AvaSphere-80 (Avantes) with calibration lamp (NIST standard accuracy). The colorimetric data were taken by Avas-pec-ULS2048XL (Avantes) detector. Colorimetric data for polymers on ITO were obtained according to CIE (the Commission Internationale de I'Eclairege – International Commission on Illumination) method developed in 1976. DFT calculations were carried out with B3LYP [44–46] hybrid functional with a 6-31G(d) basis set. The ground state geometry was optimized without symmetry constrains to a local minimum, which was followed by frequency calculations. No imaginary frequencies were detected, which proved that obtained geometry was a local minimum. All the calculations were carried out with polarizable continuum model [47], using dichloromethane as a solvent to simulate the solution effects. All the calculations were carried out with Gaussian 09 software [48]. The input files and plots were prepared with Gabedit [49] software.

3. Results and Discussion

We started an investigation of the compounds from Cyclic Voltammetric analysis Fig. 2. The compounds (**1-3**) undergo multistep oxidation processes showing similar positions for the first two oxidation signals. Firstly, the two signals show reversible or quasi-reversible redox coupling, visible on the CV curves (Fig. 2b). The position of the redox peaks, where the distance

between them is around 0.5 V, is characteristic for triphenylamine derivatives [50] when the unsubstituted part of TPA forms dimeric structures, resulting in a triphenylbenzidine moiety [51,52]. The potential range between 0.7–1.5 V shows the next oxidation processes, with their characteristics dependent upon the molecular structure. Compound **1** shows a doublet oxidation peak at potentials 0.9 and 1.1 V, while compound **2** shows only one oxidation peak at 0.8 V. Compound **3** shows a multielectron process, with the high peak evidence of follow-up reactions resulting in electroactive products. The first two oxidation peaks of

Table 1
Electrochemical and optical band-gap characteristics.

Compound	E_{Ox} [V][a]	E_{Red} [V][b]	IP [eV][c]	EA [eV][d]	E_G^{el} [eV][e]	E_G^{op} [eV][f]
1	0.13	−2.91	−5.23	−2.19	3.04	2.95
2	0.15	−2.78	−5.25	−2.32	2.93	2.83
poly(2)	0.03	–	−5.13	−2.53	–	2.60
3	0.14	−2.68	−5.24	−2.42	2.82	2.80
poly(3)	0.10	–	−5.20	−2.70	–	2.50

[a] The first oxidation potentials of compounds and polymers from CV measurements.

[b] The first reduction potentials of compounds and polymers from CV measurements.

[c] IP calculated by the formula IP = −(E_p + 5.1), where E_p is onset of CV oxidation potential versus Fc/Fc$^+$ [58–63].

[d] Energy of EA calculated by the formula EA = −(E_n + 5.1), where E_n is onset of CV reduction potential versus Fc/Fc$^+$, in the case of polymers the EA is taken from subtraction of optical gap from IP as polymers were dissolving/degrading in THF [58–65].

[e] Energy of band-gap calculated from the difference between IP and EA.

[f] Energy of band-gap calculated from UV–vis spectroscopy data $E_G^{op} = hc/\lambda_{onset}$, where h is Planck's constant, c is speed of light in a vacuum, λ_{onset} is polymer onset of absorption [58,62,63,65].
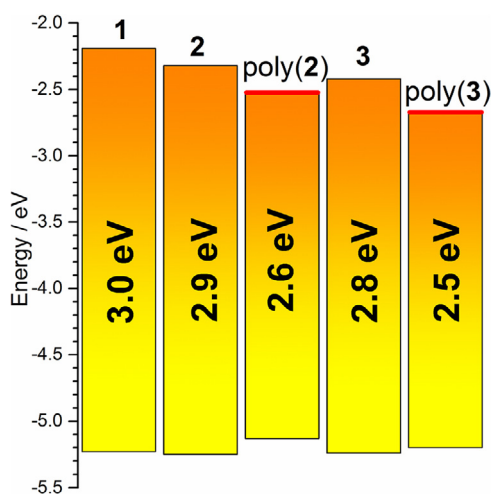
Fig. 4. Energy diagram of IP and EA levels of investigated molecules **1**-**3** and electrodeposited films poly(**2**) and poly(**3**).

a radical cation. The oxidation potential of TPA depends upon the substituents attached to the aromatic rings [54]. When the TPA's para positions are free, the radical cation may dimerize resulting in the creation of new tetraarylbenzidine structures [55].

The small changes in the onset potentials of the first oxidation peaks of all compounds could be related to differences in the para substituents on the TPA core, where a methoxy group stabilizes the TPA radical cation. The second process was found to be quasi-reversible (Fig. 2**b**), but during CV formation of new species on or near the electrode was not observed.

The third oxidation process of compound **1** was found to be irreversible (Fig. 3) and during multiple scans, only a small deviation in signal intensity was observed. This might suggest that the products of the electrochemical reaction were soluble in the solvent and therefore did not cover the electrode. During multiple scans, oxidation of compounds **2** and **3** started at lower potentials and the current grew overtime, which usually means that the electrodes were covered with new electroconductive layers of poly (**2**) and poly(**3**). We observe that during this process both of the TPA redox systems are conserved and between them a new peak is formed around 0.4 V. This new peak could be associated with electrohydrodimerization process of unsubstituted para position on the phenyl ring in the hydrazone moiety and the formation of a benzidine derivative. The oxidation process associated with the benzidine derivative is well known in literature [56,57]. Compound **1** has only one phenyl ring, so only soluble dimers maybe formed. Compound **2** has two phenyl groups and therefore a linear polymer could be formed, while for compound **3** a branched structure could be obtained.
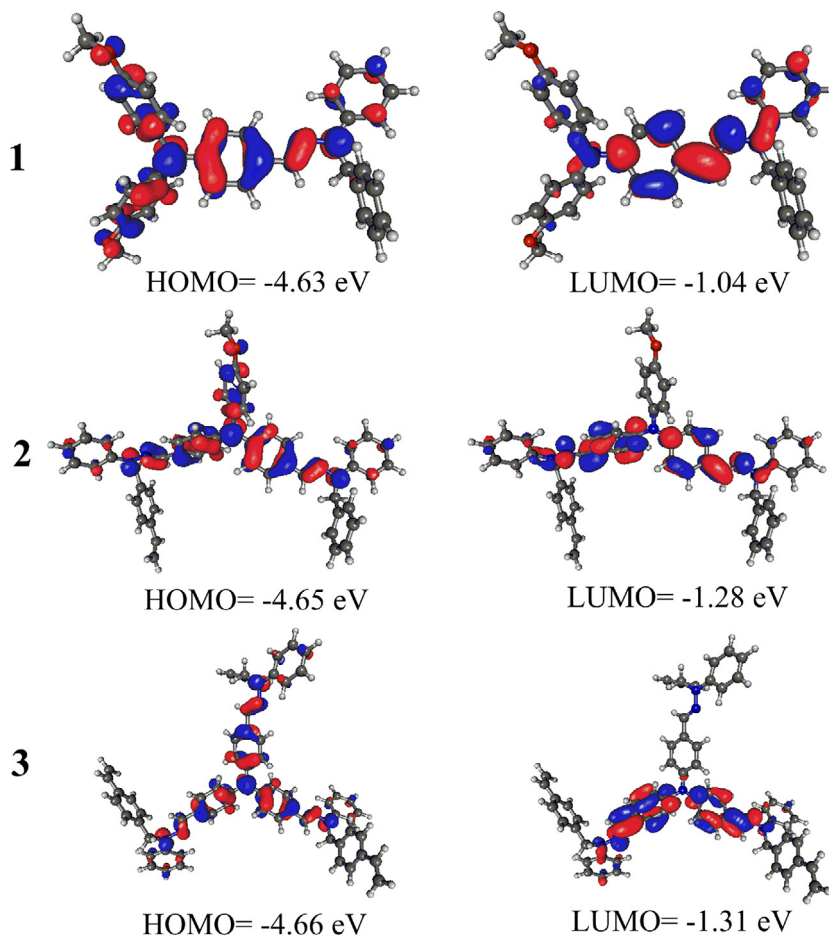
each compound were investigated further using cyclic voltammetry. These measurements show that when the upper potential is below +0.4 V, there is no change in the voltammetric curves, which highlights the reversibility of first redox couple. Such behaviour suggests the first redox couple is responsible for the process held on the triphenylamine group. Such a process is well known in the literature [53] and is related to the oxidation of the TPA unit to form

Fig. 5. The frontier molecular orbitals of the investigated molecules: compounds **1**, **2** and **3**.

Table 2
The calculated energies of frontier molecular orbitals and band-gaps.

Compound	E_{IP} [eV]	E_{EA} [eV]	E_G^{calc} [eV]
1	−4.63	−1.04	3.59
2	−4.65	−1.28	3.39
3	−4.66	−1.31	3.35
dimer of **1**	−4.53	−1.19	3.34
dimer of **2**	−4.57	−1.34	3.23
dimer of **3**	−4.59	−1.39	3.20

A decrease of oxidation onset potentials suggests that the new species formed on the electrode surface possess more extended conjugation than the initial compounds.

The CV curves of compound **2** and **3** (Fig. 3**b**) show a regular increase of the layer thickness deposited on the electrode, shown by a decreasing onset, which proves an increase of conjugation length after every cycle. The reduction peak only slightly shifts to the lower potentials with successive cycles, which suggests quite good conductivity of the layer and rather a fast ion movement. Poly (**2**) and poly(**3**) were studied by the CV technique in monomer-free solutions. Both received polymers were characterized by three redox systems where their potential depends on polymer structure. Poly(**2**) has a first oxidation potential of the triphenyl-amine centre (to radical cation) at lower potential than for poly(**3**), where the redox of the third process (oxidation of DPA polaron to bipolaron) we observe opposite behaviour. The second oxidation peak remains at the same position. Such behaviour could be related to changes in the polymer structure, where poly(**2**), may be linear and poly(**3**), branched. Branched or crosslinked polymers are difficult to dope (or dedope), which could elevate the first oxidation potential as the counter ion movement is disturbed. After relaxation of the oxidized structure higher oxidation centres are easier to approach. The onsets of oxidation and reduction processes were estimated from the electrochemical analysis, and

these values were used to calculate ionization potential (IP) and electron affinity (EA) energies (Table 1).

The band-gaps of polymers formed on electrode were found to be lower by ca. 0.3 eV compared with band-gaps of the corresponding compounds. IP-EA value of polymers were inside band-gap of their compounds which mean both IP and EA molecules were affected during the electropolymerization (Fig. 4).

There are two functionalities of the compounds which can take part in the polymerization. One is a vinyl group and the second one is unoccupied *p*-position of the phenyl ring. The electropolymerization of vinyl groups would form nonconductive species, therefore there is only a possibility of polymerization via phenyl rings with the formation of biphenyl linkages.

The further characterization of compounds **1**-**3** was done by simulating their ground-state electronic structures by DFT method using the B3LYP functional and 6-31G(d) basis set. The frontier molecular orbitals of the investigated compounds are presented in Fig. 5.

The energies of the frontier molecular orbitals of compounds **1**-**3** are presented in Table 2. The electron density of the HOMO of compounds **1**-**3** is localized on the triphenylamine moiety extending to the hydrazone group, showing a high degree of conjugation in the compounds. Nevertheless, the number of hydrazine groups in a compound does not affect the energy of the HOMO level, being almost equal in all cases. The LUMO level is more localized, expanding only to two arms of the compounds. Furthermore, for compound **1,** the LUMO is higher by 0.25 eV, compared to **2** and **3**.

Calculations were also performed for the dimers of investigated compounds, assuming that during electrochemical oxidation coupling of the charged forms takes place on the phenyl rings (Fig. 6).

The calculations revealed that both HOMO and LUMO levels are spread between the triphenylamine moieties of units through the
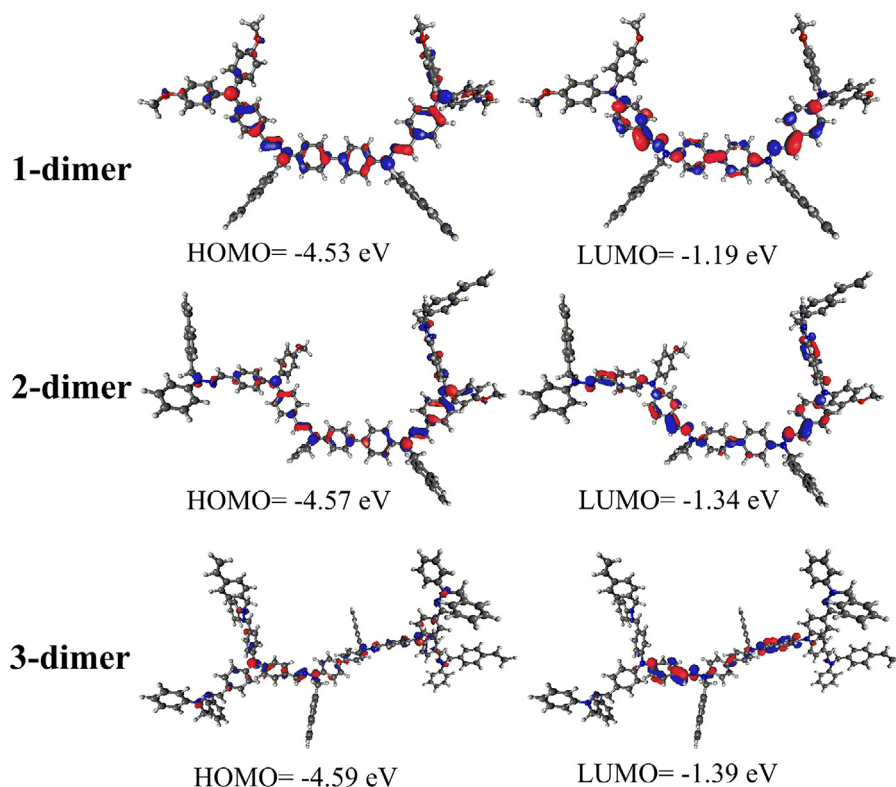

1-dimer   HOMO= -4.53 eV   LUMO= -1.19 eV

2-dimer   HOMO= -4.57 eV   LUMO= -1.34 eV

3-dimer   HOMO= -4.59 eV   LUMO= -1.39 eV

Fig. 6. The molecular orbitals and energies of the dimer of compounds **1, 2** and **3**.

biphenyl linker. These results indicate that conjugation between two sides of the dimer is present.

The IR spectroelectrochemical tools were used for the investigation of the structures of compounds and polymers during doping (Fig. 7). The differential spectra were recorded taking the tested compound as a reference. The changes occurring during polymerization were analyzed; disappearing chemical groups were characterized by the positive peaks (increasing of transmittance) and the newly appearing groups were characterized by the negative peaks (decreasing of transmittance) (Fig. 7**b,c**).

The IR spectra of the investigated compounds (**1-3**) are shown in Fig. 7**a**. The characteristic signals at 826 cm^{-1} attributed to disubstituted benzene rings are present in the spectra of all the studied compounds. The signals at 750 and 689 cm^{-1} in the spectrum of compound **2** are very weak comparing with the intensity of the corresponding signals in the spectrum of compound **3** and in the spectrum of **1** they do not appear at all. The other difference observed in the investigated spectra is related to the signal of methoxy group (1243 cm^{-1}). The strong signal is observed in the spectrum of **1**, for **2** this signal is weaker ant it does not exist in the spectrum of **3**.

The spectra recorded during the electropolymerization of compound **2** are shown in Fig. 7**b**. During the polymerization process the changes in the IR spectra occurring at around 1580 cm^{-1} proving disappearance of the double bonds. The most important changes are in the region from 700 to 900 cm^{-1}. The increase of the transmittance at 760 and 678 cm^{-1} shows the disappearance of the monosubstituted benzene rings.
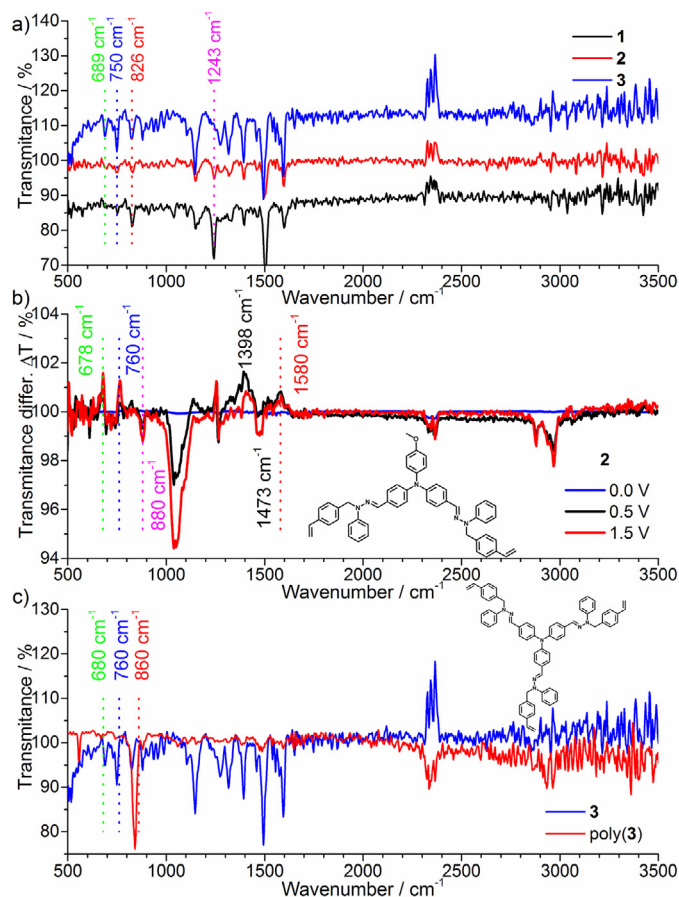

Fig. 7. IR spectra of all molecules (a), IR spectra recorded during potentiostatic electrochemical oxidation of **2** (b) and IR spectra of **3** and poly(3) film (c). (For interpretation of the references to colour in the text, the reader is referred to the web version of this article.)

Simultaneously, the intensity of the signal of disubstituted rings at around 880 cm^{-1} increases.

In the case of compound **3**, spectra of the monomer (Fig. 7c blue line) and the polymer deposited on the electrode (Fig. 7c red line) were compared. By direct comparison of the spectra, we observe substantial differences in the range related to the changes of monosubstituted phenyl group (650–900 cm^{-1}). Additionally, we observe the disappearance of two peaks at 680 cm^{-1} and 760 cm^{-1} in the monomer and the appearance of a new peak at 860 cm^{-1} in the polymer, suggesting the para substitution of our monosubstituted phenyl group.

It can be presumed on the basis of IR spectroelectrochemical studies, that polymerization occurs due to the reaction of vinyl groups with the unsubstituted positions of the benzene ring or due to the reaction of two phenyl moieties. Taking into consideration that the reaction of the vinyl group and benzene ring does not result in the formation of conjugated species, one can suggest that electropolymerization occurs mainly due to "dimerization" of phenyl rings. This observation was proven by the electrochemical investigation, where during polymerization we observe the formation of a new (third) redox centre between the previous two oxidation peaks of PDA by forming a benzidine-type structure by two para-substituted phenyl rings.

The UV-Vis-NIR spectroelectrochemical technique was used to analyze the products of the electrochemical reactions (Figs. 8 and 9). Using this method it was found that well-defined triarylamine radical cation bands were formed during the oxidation of compound **1** (Fig. 8**a**). Reduction of the neutral compound peak (375 nm) was observed during oxidation while new bands occurred in the ranges of 400–600 nm, 600–790 nm, and 900–1600 nm. After the reduction process, the shape of the spectrum was found to be similar to the spectrum of the neutral compound without any new bands, proving the reversibility of electrochemical process and lack of subsequent chemical reactions.

The spectra of the oxidized compound **2** revealed disappearance of the absorption peak of the neutral compound (400 nm) and formation of new broad radical cation bands in the ranges of 450–600 nm, 800–1100 nm and 1100–1700 nm. At the second oxidation process, the peak-less band appeared in the range from 600 to 750 nm. At higher potentials, peak-less bands were observed in the whole spectral range that can be explained by the formation of the oxidized polymer on the electrode. The spectra of the neutral polymer are shown in Fig. 9a, where a new absorption band is formed in the range between 460–580 nm. The formation of this new absorption band at a higher wavelength than the monomer proves the formation of a higher conjugated structure inside the polymer net. The optical band gap data of monomers and polymers are found in Table 1. The similar behavior was discovered for compound **3,** and the formation of polymer on the electrode was observed.

Polymers poly(**2**) and poly(**3**) formed on ITO electrode were investigated using monomer free electrolyte (Fig. 9). During the oxidation of poly(**2**), the decrease of the intensity of the neutral polymer peak was observed, and new polaronic bands (450–600 nm, 800–1700 nm) were formed. The isosbestic point was well preserved which suggests the absence of side reactions. At the higher potentials, new bipolaronic bands were formed in the ranges of 500–800 nm and 1100–1600 nm.

The similar changes but less obvious were observed in spectra of poly(**3**) during electrochemical oxidation. At higher potentials, one band with two bipolaronic peaks at 600 nm and 720 nm were formed while the polaronic band at 900–1700 nm disappeared. This observation shows that the polarons undergo the follow-up reaction (polarons → bipolarons) with much higher rate than they are created from the neutral polymer.
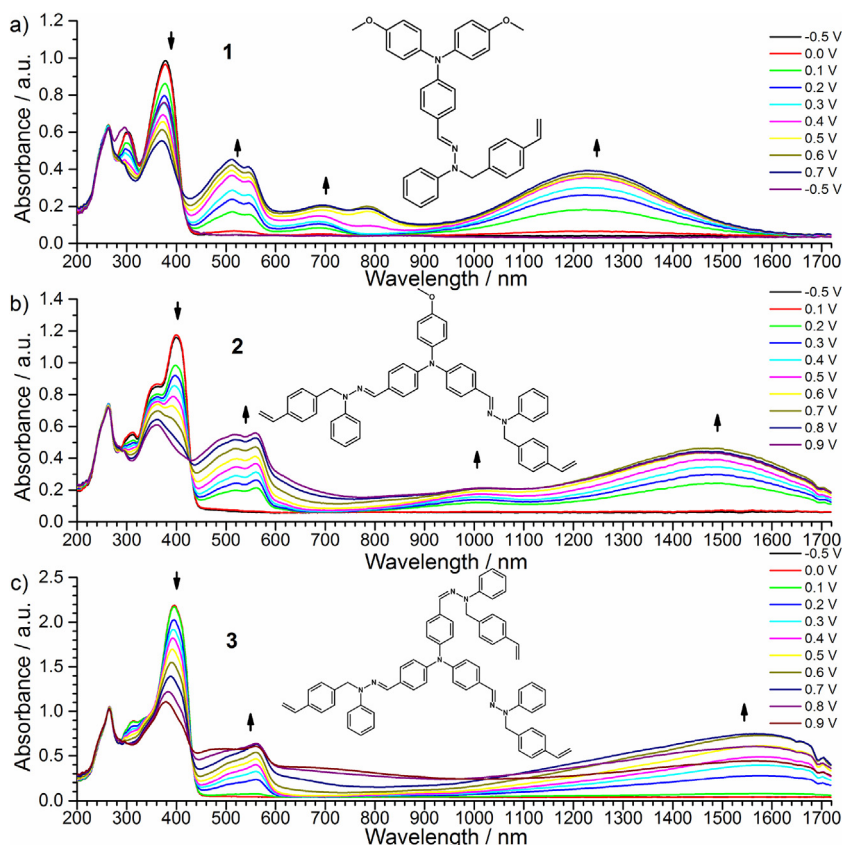
Fig. 8. UV–vis spectra recorded during potentiostatic electrochemical oxidation of the compounds. The black line denotes the starting potential; all potentials vs Fc/Fc⁺ redox couple.
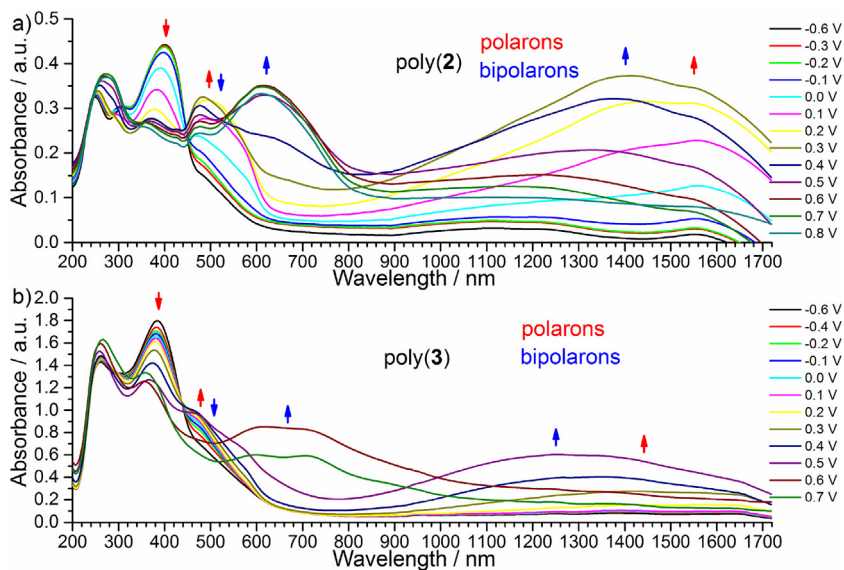

Fig. 9. UV–vis spectra recorded during potentiostatic electrochemical oxidation of polymers. Arrows show increase and decrease of absorption bands during the formation of polaron and bipolaron species. The black line denotes the starting potential; all potentials vs Fc/Fc⁺ redox couple.

The potentiodynamic UV–vis spectroelectrochemistry of polymers was employed for the investigation of poly(**2**) and poly(**3**) (Figs. 10 and 11). During doping of poly, (**2**) well-defined two isosbestic points were observed at 443 nm and 521 nm. The first isosbestic point is assigned to the oxidation of neutral polymer to the polaron and the second peak is ascribed to the bipolaron

formation from polaron (Fig. 10**a**). Bipolarons were formed almost instantly together with polarons. After 20 seconds (ca. 0.5 V) the number of polaronic species decreased. This observation shows that the rate of the reaction of formation of bipolarons is much higher than that of the formation of polarons (Fig. 10**b**). Derivative of absorbance change of reveal a good correlation with CV curve.
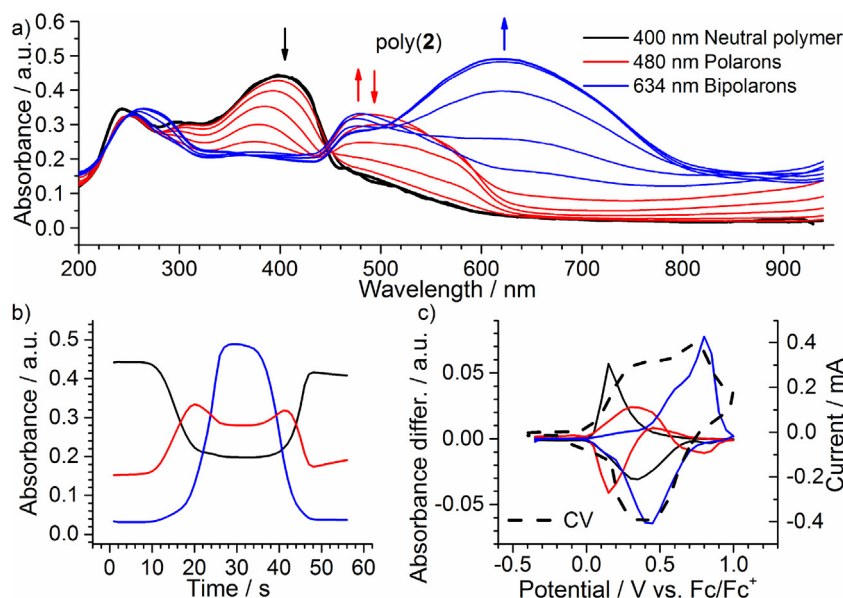
Fig. 10. Potentiodynamic UV-Vis-NIR spectra recorded during electrochemical oxidation of polymer poly(**2**); b) and c) show the absorbance change at the wavelengths of neutral polymer (black line), polaron (red line), bipolaron (blue line); dashed line shows CV curve. Scan rate 0.05 V·s^{-1}, dichloromethane solution. All potentials vs Fc/Fc$^+$ redox couple. (For interpretation of the references to colour in this figure legend, the reader is referred to the web version of this article.)
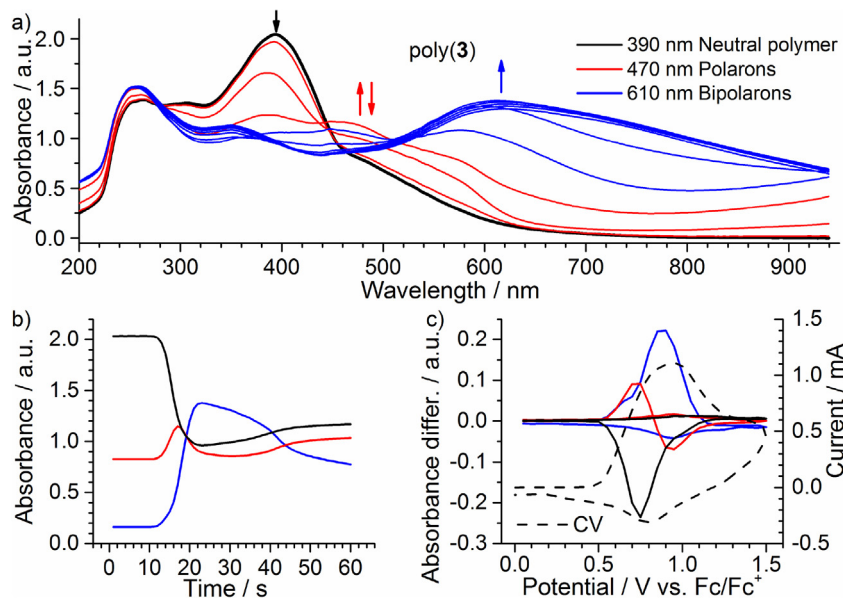

Fig. 11. Potentiodynamic UV-Vis-NIR spectra recorded during electrochemical oxidation of polymer poly(**3**), b) and c) show absorbance changes at wavelengths of neutral polymer (black line), polaron (red line), bipolaron (blue line); dashed line shows CV curve. Scan rate 0.05 V·s^{-1}, dichloromethane solution. All potentials vs Fc/Fc$^+$ redox couple. (For interpretation of the references to colour in this figure legend, the reader is referred to the web version of this article.)

The oxidation peaks at 0.3 V and 0.75 V are assigned to the polaronic and bipolaronic process, respectively (Fig. 10c).

The similar changes in the absorbance spectra were observed for the oxidized poly(**3**) (Fig. 11). During doping, "overoxidation" process was observed at the potentials above 1.0 V (Fig. 11b,c). The small changes during dedoping process occurred, and the original spectra were not observed. In the similar like for poly(**2**), it was possible to find similar behavior of voltabsorptiometric peaks and the curves of CV process (Fig. 11c).

In order to gain information on the products of electrochemical reactions, EPR spectroelectrochemical measurements were carried out. In the case of compound **1**, application of the potential of 0.20 V vs. Fc/Fc$^+$ leads to the formation of a compound with unpaired spin (Fig. 12a). G-factor of the obtained radical cation was found to be 2.00326, which suggest that the spin density is located mainly on the nitrogen atom. Since this potential is typical for the oxidation of triphenylamine moiety, it can assume that its nitrogen atom is responsible for the localization of spin. EPR spectra exhibit hyperfine structure, however due to the large width of the signal, it is poorly split, which makes it difficult to identify the structure of radical cation. The radical cation number rises up during the oxidation, having its maximum by the first oxidation peak.
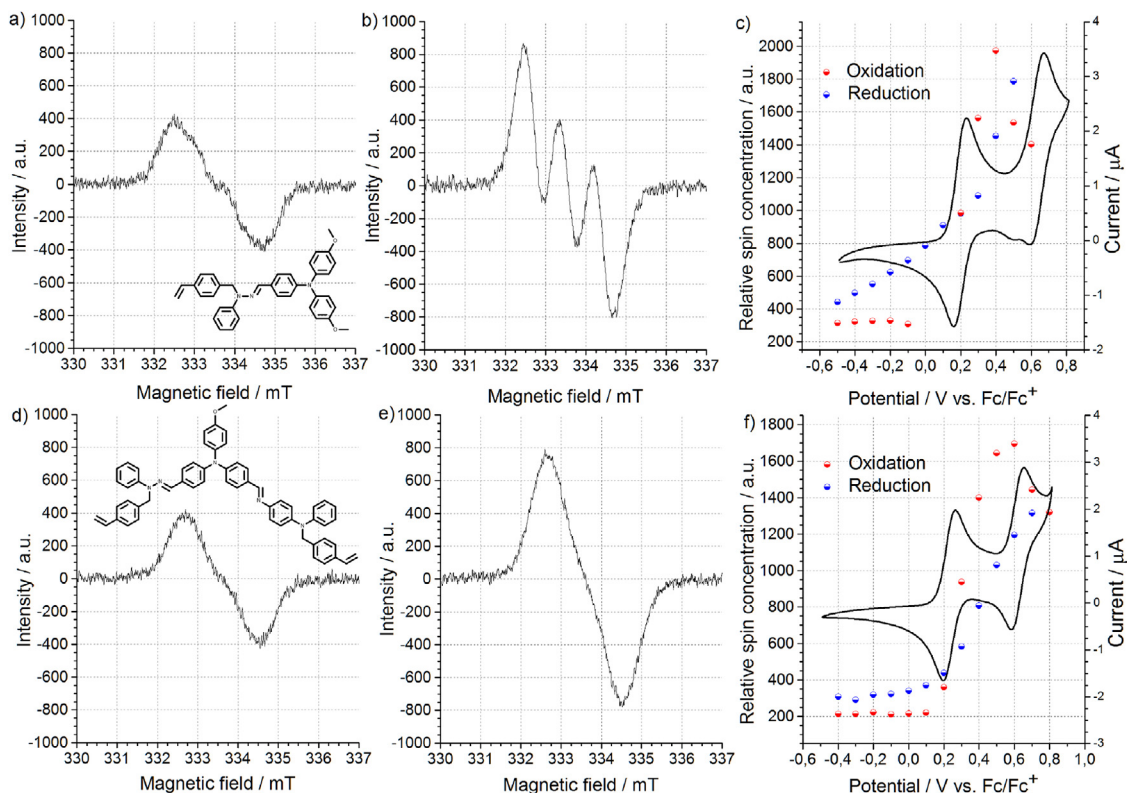
Fig. 12. a) EPR signal at first oxidation peak of compounds **1**, b) EPR signal at second oxidation peak of compounds **1**, c) change of spin concentration during oxidation/reduction of compound **1**, compared with CV curve, d) EPR signal at first oxidation peak of compounds **2**, e) EPR signal at second oxidation peak of compounds **2**, f) change of spin concentration during oxidation/reduction of compound **2**, compared with CV curve.
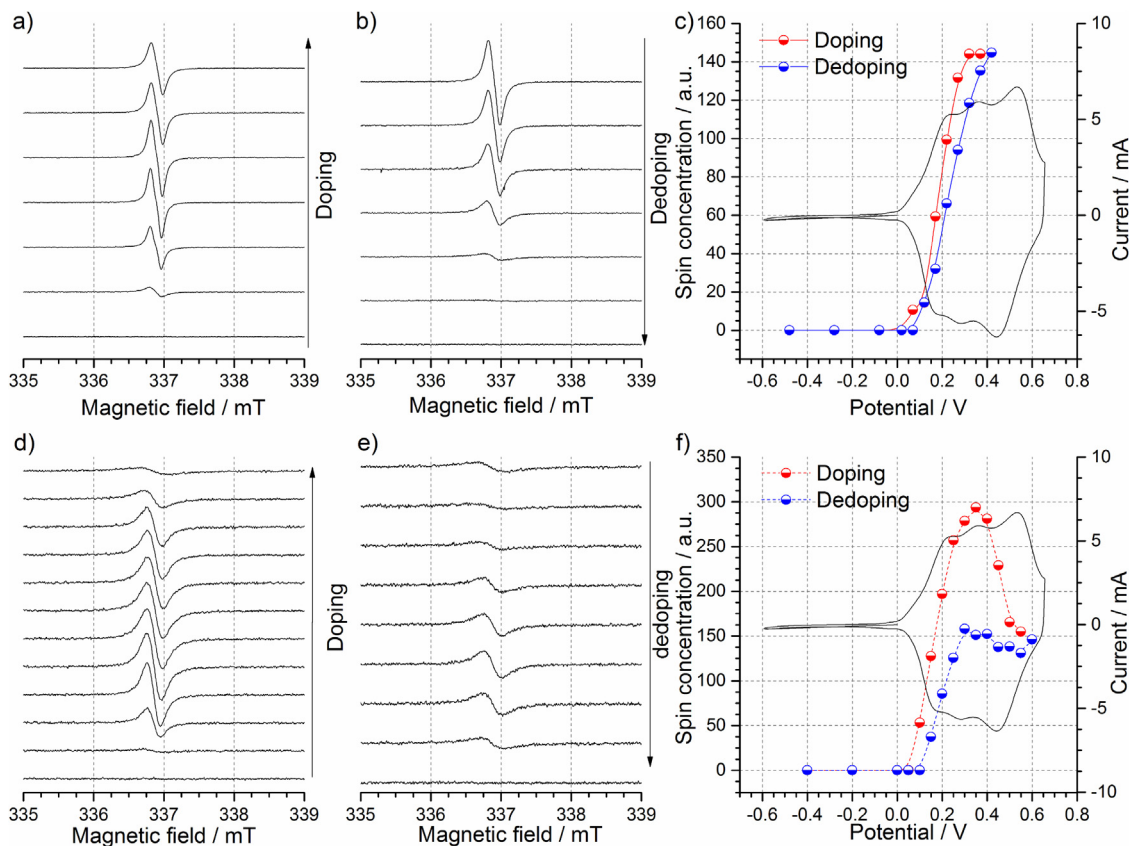

Fig. 13. EPR spectra of polymer poly(**3**) a) EPR signal during doping till second oxidation peak, b) EPR signal during dedoping, c) Spin concentration change with voltage, compared with CV curve, d) EPR signal during doping till third oxidation peak, e) EPR signal during dedoping, f) Spin concentration change with voltage, compared with CV curve.

Application of the potential of the second oxidation peak is usually associated with the formation of the dication, which as a spinless species should not be detected by EPR spectroscopy. However, in the case of compound **1** after polarization of the working electrode to potential of 0.60 V vs. Fc/Fc$^+$ one can still observe an EPR spectrum (Fig. 12**b**), however with a lower total number of radicals, compared to its maximum concentration (Fig. 12**c**). This observation can lead to the conclusion that dication formed during the electrochemical reaction reacts with the neutral molecule, yielding radical cations. The value of the g-factor (2.00353) and the triplet structure of the spectra suggest that the spins are located on the nitrogen atoms of the triarylamine moiety.

In the case of the compound, **2** evolution of EPR spectra was found to be similar to that of compound **1** (Fig. 12**d**), a decrease radical number is seen after applying the potential of the second oxidation peak (Fig. 12**f**). The difference was observed in the shape of the EPR spectra for the second oxidation peak. EPR spectra was not well-defined, which is caused by the higher delocalization on a much larger π-conjugated system of **2** (Fig. 12**e**).

The doping process of poly(**3**) was investigated in two potential ranges to observe the formation of charge carriers (Fig. 13). During the oxidation of the compound in the lower potential range, we observed the formation of polaronic species with quite a strong EPR peak (Fig. 13**a**). Since the potential of first oxidation peak of polymer coincidences with the monomer, one can assume that TPA moieties are oxidized. Second oxidation peak of poly(**3**) is not

present in the CV of monomer **3**, therefore involves oxidation of benzidine moiety created during electropolymerization. In the dedoping stage, the whole charge was neutralized, and no residual EPR signals were observed (Fig. 13**b**).

When higher potentials were applied, the disappearance of EPR signal was observed. This observation can be explained by the formation of spin-less bipolaronic (Fig. 13**d**). EPR signal reappeared during the dedoping process, however, EPR signal were still observed after reduction (Fig. 13**e**). The spin concentration behavior suggests that the third polymer oxidation peak is predetermined by the bipolaron formation process on both TPA and benzidine moiety (Fig. 13**f**).

Dynamic electrochemical impedance spectroscopy (DEIS) was used for characterization of the conductivity of the obtained polymers. During CV process, (Fig. 3**d**) impedance analysis was performed with the scan rate 1 mV/s. During the redox process, the clear change changes in the impedance spectra of poly(**2**) and poly(**3**) were observed (Fig. 14). To analyze the impedance spectroscopy data in more detail, the equivalent circuit was made. As it is shown in Fig. 14, equivalent circuitry was used for fitting the Nyquist curves for the covered electrode. In this circuit corresponding to the oxidation and reduction processes of the polymer layers on the electrode, one can propose $(R_1(Q_1(R_2W))(Q_2R_3))$, where R_1 is the solution resistance, R_3 is the resistance to charge transfer of the metal and R_2 is the resistance of a layer of a polymer. Q is a solid phase element (CPE) in which n is the number of electrons
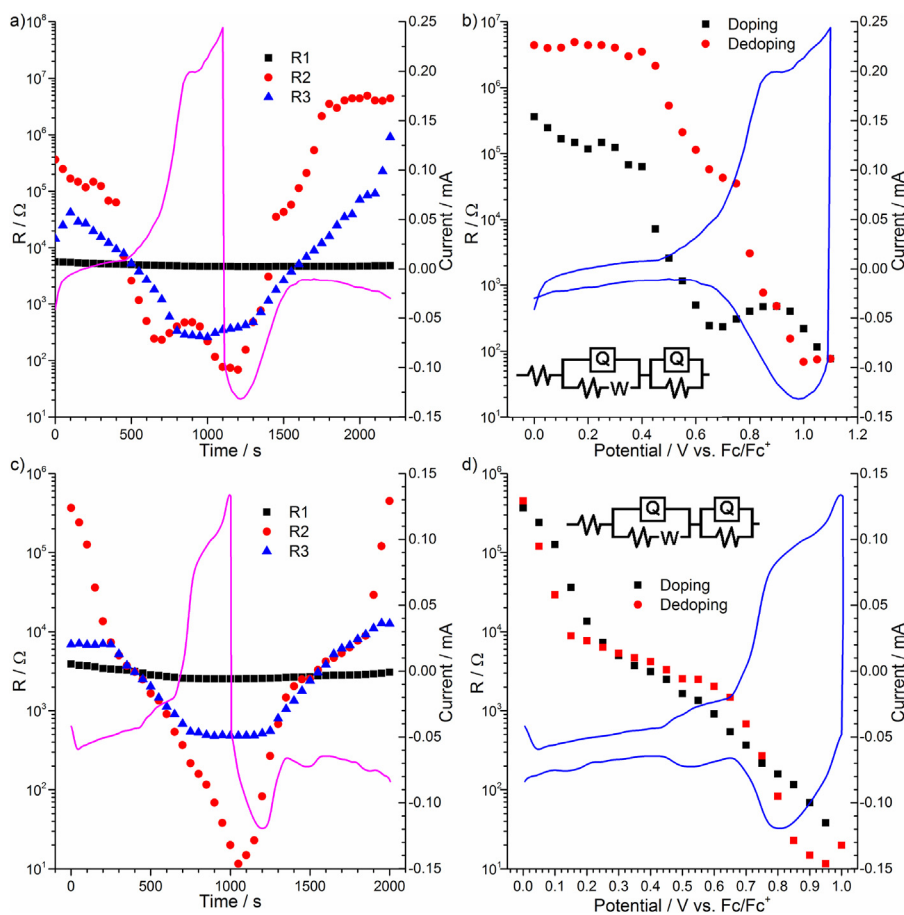

Fig. 14. DEIS spectroelectrochemistry data for polymers poly(**2**) and poly(**3**). Sample concentration 10^{-3} M, scan rate 0.001 V·s^{-1}, dichloromethane solution. All potentials vs Fc/Fc$^+$ redox couple.

exchanged at the interface of electrode/solution. Here, n may adopt values between 0 and 1. For Q_1 the n value was stable at 1 but for Q_2 it varied between 0.8 (for doped poly(**2**)) or 0.65 (for doped poly (**3**)) and 1 (for the neutral polymers). Warburg impedance was also observed in the curves originating from the diffusion of counter ions inside the polymer layer.

The changes in the polymer layer were observed by DEIS, during oxidation the resistivity of polymer decrease (Fig. 14). Resistance was restored during dedoping process which suggested good stability of polymers.

4. Conclusions

Electropolymerization of triphenylamine-based hydrazones containing reactive vinylbenzyl groups was studied by electrochemical and spectroelectrochemical tools. All the investigated compounds exhibited multielectrochromic properties and compound **3** showed the highest change of absorbance which should be useful in electrochromic windows application.

The disappearance of the monosubstituted phenyl rings and formation of bisubstituted species was proved using IR spectroscopy. In addition, the IR spectroelectrochemistry demonstrates electropolymerization process via "dimerization" of phenyl rings. It was possible to demonstrate that using spectroelectrochemical methods it is possible to find reaction side of the compound and estimate the polymer structure.

The EPR spectroelectrochemistry showed the formation of stable polarons in compound **1** which decreased the possibility of dimerization.

Compounds **2** and **3** electropolymerized during the third oxidation process and the obtained polymers were found to be electroactive. The polymers were stable below 1.0 V and during doping polarons and bipolarons were formed as charge carriers. Both polymers were found to be electrochemically active and showed electrochromic properties. The electrochromism of polymer poly(**2**) was fully reversible.

Acknowledgments

References

[1] M. Hidai, Y. Mizobe, Recent Advances in the Chemistry of Dinitrogen Complexes, Chem. Rev. 95 (1995) 1115.

[2] R. Lazny, A. Nodzewska, N,N-Dialkylhydrazones in Organic Synthesis. From Simple N,N-Dimethylhydrazones to Supported Chiral Auxiliaries, Chem. Rev. 110 (2010) 1386.

[3] S. Kobayashi, Y. Mori, J.S. Fossey, M.M. Salter, Catalytic enantioselective formation of C-C bonds by addition to imines and hydrazones: a ten-year update, Chem. Rev. 111 (2011) 2626.

[4] J.-M. Lehn, From supramolecular chemistry towards constitutional dynamic chemistry and adaptive chemistry, Chem. Soc. Rev. 36 (2007) 151.

[5] J.-M. Lehn, Constitutional Dynamic Chemistry: Bridge from Supramolecular Chemistry to Adaptive Chemistry, Springer, 2012.

[6] J.-M. Lehn, Perspectives in Chemistry—Steps towards Complex Matter, Angew. Chem. Int. Ed. 52 (2013) 2836.

[7] P. Vicini, F. Zani, P. Cozzini, I. Doytchinova, Hydrazones of 1,2-benzisothiazole hydrazides: synthesis, antimicrobial activity and QSAR investigations, Eur. J. Med. Chem. 37 (2002) 553.

[8] C. Loncle, J. Brunel, N. Vidal, M. Dherbomez, Y. Letourneux, Synthesis and antifungal activity of cholesterol-hydrazone derivatives, Eur. J. Med. Chem. 39 (2004) 1067.

[9] A. Masunari, L.C. Tavares, A new class of nifuroxazide analogues: Synthesis of 5-nitrothiophene derivatives with antimicrobial activity against multidrug-resistant Staphylococcus aureus, Bioorg. Med. Chem. 15 (2007) 4229.

[10] P. Vicini, M. Incerti, P. La Colla, R. Loddo, Anti-HIV evaluation of benzo[d] isothiazole hydrazones, Eur. J. Med. Chem. 44 (2009) 1801.

[11] R. Raue, A. Brack, K. Lange, Salt-free Synthesis of Azo and Hydrazone Dyes Under CO_2 Pressure, Angew. Chem. Int. Ed. 30 (1991) 1643.

[12] P. Shen, X. Liu, S. Jiang, Y. Huang, L. Yi, B. Zhao, S. Tan, Effects of aromatic π-conjugated bridges on optical and photovoltaic properties of N,N-diphenylhydrazone-based metal-free organic dyes, Org. Electron. 12 (2011) 1992.

[13] V. Getautis, M. Daskeviciene, V. Gaidelis, V. Jankauskas, New branched hydrazones as hole transporting materials, J. Photochem. Photobiol. A: Chem 175 (2005) 39.

[14] R. Lygaitis, V. Getautis, J.V. Grazulevicius, Hole-transporting hydrazones, Chem. Soc. Rev. 37 (2008) 770.

[15] O.-P. Kwon, M. Jazbinsek, H. Yun, J.-I. Seo, E.-M. Kim, Y.-S. Lee, P. Gunter, Pyrrole-Based Hydrazone Organic Nonlinear Optical Crystals and Their Polymorphs, Cryst. Growth Des. 8 (2008) 4021.

[16] F.J. Uribe-Romo, C.J. Doonan, H. Furukawa, K. Oisaki, O.M. Yaghi, Crystalline Covalent Organic Frameworks with Hydrazone Linkages, J. Am. Chem. Soc. 133 (2011) 11478.

[17] X.-P. Zhou, Y. Wu, D. Li, Polyhedral metal-imidazolate cages: control of self-assembly and cage to cage transformation, J. Am. Chem. Soc. 135 (2013) 16062.

[18] D.N. Bunck, W.R. Dichtel, Bulk synthesis of exfoliated 2D polymers using hydrazone-linked covalent organic frameworks, J. Am. Chem. Soc. 135 (2013) 14952.

[19] X. Su, I. Aprahamian, Hydrazone-based switches, metallo-assemblies and sensors, Chem. Soc. Rev. 43 (2014) 1963.

[20] S. Rowan, S. Cantrill, G. Cousins, J. Sanders, J. Stoddart, Dynamic covalent chemistry, Angew. Chem. Int. Ed. 41 (2002) 898.

[21] P.T. Corbett, J. Leclaire, L. Vial, K.R. West, J.-L. Wietor, J.K.M. Sanders, S. Otto, Dynamic combinatorial chemistry, Chem. Rev. 106 (2006) 3652.

[22] Y. Jin, C. Yu, R.J. Denman, W. Zhang, Recent advances in dynamic covalent chemistry, Chem. Soc. Rev. 42 (2013) 6634.

[23] M. Juozapavicius, B.C. O'Regan, A.Y. Anderson, J.V. Grazulevicius, V. Mimaite, Efficient dye regeneration in solid-state dye-sensitized solar cells fabricated with melt processed hole conductors, Org. Electron. 13 (2012) 23.

[24] L.A. Tatum, X. Su, I. Aprahamian, Simple Hydrazone Building Blocks for Complicated Functional Materials, Acc. Chem. Res. (2014) 2141.

[25] F.R. Japp, F. Klingemann, Ueber die Constitution einiger sogenannten gemischten Azoverbindungen, Justus Liebigs Ann. Chem. 247 (1888) 190.

[26] G. Stork, J. Benaim, Monoalkylation of α,β-unsaturated ketones via metalloenamines: 1-butyl-10methyl Δ1(9)-2-octalone, Org. Synth. 57 (1977) 69.

[27] V. Lefebvre, T. Cailly, F. Fabis, S. Rault, Two-Step Synthesis of Substituted 3-Aminoindazoles from 2-Bromobenzonitriles, J. Org. Chem. 75 (2010) 2730.

[28] P.M. Borsenberger, Hole transport inp-diethylamino-benzaldehyde-diphenyl hydrazine, Adv. Mater. Opt. Electron. 1 (1992) 73.

[29] S. Nomura, K. Nishimura, Y. Shirota, Charge Transport in the Supercooled Liquid State of Arylaldehyde Hydrazones, Mol. Cryst. Liq. Cryst. 313 (1998) 247.

[30] G.V. Getautis, M. Daskeviciene, T. Malinauskas, V. Gaidelis, V. Jankauskas, Z. Tokarski, Cross-linkable hydrazone-containing molecular glasses for electrophotography, Synthetic Met. 155 (2005) 599.

[31] V. Mimaite, J.V. Grazulevicius, J. Ostrauskaite, V. Jankauskas, Synthesis and properties of triphenylamine-based hydrazones with reactive vinyl groups, Dyes Pigments 95 (2012) 47.

[32] V. Getautis, J.V. Grazulevicius, T. Malinauskas, V. Jankauskas, Z. Tokarski, N. Jubran, Novel Families of Hole-Transporting Monomers and Polymers, Chem. Lett. 33 (2004) 1336.

[33] V. Getautis, J.V. Grazulevicius, M. Daskeviciene, T. Malinauskas, D. Jankunaite, V. Gaidelis, V. Jankauskas, J. Sidaravicius, Z. Tokarski, Novel hydrazone based polymers as hole transporting materials, Polymer 46 (2005) 7918.

[34] V. Getautis, J.V. Grazulevicius, M. Daskeviciene, T. Malinauskas, V. Jankauskas, J. Sidaravicius, A. Undzenas, Novel dihydrazone based polymers for electrophotography, Eur. Polym. J. 43 (2007) 3597.

[35] V. Getautis, O. Paliulis, I. Paulauskaite, V. Gaidelis, V. Jankauskas, J. Sidaravicius, Z. Tokarski, K. Law, N. Jubran, Crosslinkable Branched Hydrazones as Hole Transporting Materials, J. Imag. Sci. Technol. 48 (2004) 265.

[36] E. Juskelyte, R. Lygaitis, G. Buika, J. Ostrauskaite, J.V. Grazulevicius, V. Jankauskas, Glass-forming hole-transporting carbazole-based hydrazone monomers, polymers, and twin compounds, React. Funct. Polym. 70 (2010) 81.

[37] E. Andrikaityte, M. Cekaviciute, J. Simokaitiene, G. Buika, J.V. Grazulevicius, V. Rubeziene, Glass-forming 1,3-bis(carbazol-9-yl)propan-2-ol based monomers and polymers, React. Funct. Polym. 72 (2012) 11.

[38] J. Simokaitiene, A. Danilevicius, S. Grigalevicius, J.V. Grazulevicius, V. Getautis, V. Jankauskas, Phenotiazinyl-based hydrazones as new hole-transporting

materials for electrophotographic photoreceptors, Synthetic Met. 156 (2006) 926.

[39] R. Laurinaviciute, J. Ostrauskaite, J.V. Grazulevicius, V. Jankauskas, Synthesis, properties, and self-polymerization of hole- transporting carbazole-and triphenylamine-based hydrazone monomers, Des. Monomers Polym. 17 (2014) 255.

[40] A. Michaleviciute, R. Lygaitis, E. Andrikaityte, J. Ostrauskaite, J.V. Grazulevicius, V. Jankauskas, N. Pedisius, Charge-transporting 3,4-ethylenedioxythiophene-based hydrazone monomers and oligomers, Polym. Bull. 70 (2013) 1519.

[41] G. Barbey, C. Caullet, Oxydation electrochimique sur electrode de platine de la benzaldehyde diphenyl hydrazone en milieu nucleophile basique, Tetrahedron Lett. 18 (1974) 1717.

[42] B. Lameille, G. Barbey, C. Caullet, Oxydation electrochimique de phenylhydrazones du benzaldehyde, Electrochim. Acta 29 (1984) 339.

[43] J. Pacansky, A.D. McLean, M.D. Miller, Theoretical calculations and experimental studies on the electronic structures of hydrazones and hydrazone radical cations: formaldehyde hydrazone and benzaldehyde diphenylhydrazones, J. Phys. Chem. 94 (1990) 90.

[44] C. Lee, W. Yang, R.G. Parr, Development of the Colle-Salvetti correlation-energy formula into a functional of the electron density, Phys. Rev. B. 37 (1988) 785.

[45] A.D. Becke, A new mixing of Hartree–Fock and local density-functional theories, J. Chem. Phys. 98 (1993) 1372.

[46] A.D. Becke, Density-functional thermochemistry. III. The role of exact exchange, J. Chem. Phys. 98 (1993) 5648.

[47] J. Tomasi, B. Mennucci, R. Cammi, Quantum mechanical continuum solvation models, Chem. Rev. 105 (2005) 2999.

[48] Gaussian 09, Revision D.01, M.J. Frisch, G.W. Trucks, H.B. Schlegel, G.E. Scuseria, M.A. Robb, J.R. Cheeseman, G. Scalmani, V. Barone, B. Mennucci, G.A. Petersson, H. Nakatsuji, M. Caricato, X. Li, H.P. Hratchian, A.F. Izmaylov, J. Bloino, G. Zheng, J.L. Sonnenberg, M. Hada, M. Ehara, K. Toyota, R. Fukuda, J. Hasegawa, M. Ishida, T. Nakajima, Y. Honda, O. Kitao, H. Nakai, T. Vreven, J.A. Montgomery, Jr., J.E. Peralta, F. Ogliaro, M. Bearpark, J.J. Heyd, E. Brothers, K.N. Kudin, V.N. Staroverov, R. Kobayashi, J. Normand, K. Raghavachari, A. Rendell, J.C. Burant, S.S. Iyengar, J. Tomasi, M. Cossi, N. Rega, J.M. Millam, M. Klene, J.E. Knox, J.B. Cross, V. Bakken, C. Adamo, J. Jaramillo, R. Gomperts, R.E. Stratmann, O. Yazyev, A.J. Austin, R. Cammi, C. Pomelli, J.W. Ochterski, R.L. Martin, K. Morokuma, V.G. Zakrzewski, G.A. Voth, P. Salvador, J.J. Dannenberg, S. Dapprich, A.D. Daniels, Ö. Farkas, J.B. Foresman, J.V. Ortiz, J. Cioslowski, D.J. Fox, Gaussian, Inc Wallingford CT, 2009.

[49] A.-R. Allouche, Gabedit—A graphical user interface for computational chemistry softwares, J. Comput. Chem. 32 (2011) 174.

[50] Y.C. Chung, Y.O. Su, Effects of Phenyl- and Methyl-Substituents on p-Phenylenediamine, an Electrochemical and Spectral Study, J. Chin. Chem. Soc. 56 (2009) 493.

[51] R.F. Nelson, R.N. Adams, Anodic oxidation pathways of substituted triphenylamines. II. Quantitative studies of benzidine formation, J. Am. Chem. Soc. 90 (1968) 3925.

[52] S.C. Creason, J. Wheeler, R.F. Nelson, Electrochemical and spectroscopic studies of cation radicals. I. Coupling rates of 4-substituted triphenylaminium ion, J. Org. Chem. 37 (1972) 4440.

[53] E.T. Seo, R.F. Nelson, J.M. Fritsch, L.S. Marcoux, D.W. Leedy, R.N. Adams, Anodic Oxidation Pathways of Aromatic Amines. Electrochemical and Electron Paramagnetic Resonance Studies, J. Am. Chem. Soc. 88 (1966) 3498.

[54] A. Vallat, E. Laviron, Theoretical study of ece mechanisms in thin layer linear potential sweep voltammetry, J. Electroanal. Chem. 74 (1976) 309.

[55] K.Y. Chiu, T.X. Su, J.H. Li, T.-H. Lin, G.-S. Liou, S.-H. Cheng, Novel trends of electrochemical oxidation of amino-substituted triphenylamine derivatives, J. Electroanal. Chem. 575 (2005) 95.

[56] L.F. Oldfield, J.O.M. Bockris, Reversible Oxidation-Reduction Reactions of Aromatic Amines, J. Phys. Chem. 55 (1951) 1255.

[57] H. Yang, A.J. Bard, The application of fast scan cyclic voltammetry. Mechanistic study of the initial stage of electropolymerization of aniline in aqueous solutions, J. Electroanal. Chem. 339 (1992) 423.

[58] J. Pei, W.-L. Yu, J. Ni, Y.-H. Lai, W. Huang, A.J. Heeger, Thiophene-Based Conjugated Polymers for Light-Emitting Diodes: Effect of Aryl Groups on Photoluminescence Efficiency and Redox Behavior, Macromolecules 34 (2001) 7241.

[59] M. Lapkowski, P. Data, S. Golba, J. Soloducho, A. Nowakowska-Oleksy, Unusual band-gap migration of N-alkylcarbazole-thiophene derivative, Opt. Mater. 22 (2011) 1445.

[60] S. Trasatti, The absolute electrode potential: an explanatory note, Pure Appl. Chem. 58 (1986) 955.

[61] P. Data, M. Lapkowski, R. Motyka, J. Suwinski, Influence of heteroaryl group on electrochemical and spectroscopic properties of conjugated polymers, Electrochim. Acta 83 (2012) 271.

[62] P. Data, P. Pander, M. Lapkowski, A. Swist, J. Soloducho, R.R. Reghu, J.V. Grazulevicius, Unusual properties of electropolymerized 2,7-and 3,6-carbazole derivatives, Electrochim. Acta 128 (2014) 430.

[63] J.L. Bredas, Mind the Gap!, Mater. Horiz. 1 (2014) 17.

[64] P. Data, M. Lapkowski, R. Motyka, J. Suwinski, Influence of alkyl chain on electrochemical and spectroscopic properties of polyselenophenes, Electrochim. Acta 87 (2013) 438.

[65] P. Data, M. Lapkowski, R. Motyka, J. Suwinski, A.P. Monkman, Spectroelectrochemical analysis of charge carriers as a way of improving poly (p-phenylene)-based electrochromic windows, J. Phys. Chem. C 119 (2015) 20188.